View metadata, citation and similar papers at core.ac.uk
brought to you by CORE
provided by Repository@USM

SYNTHESIS OF SILICON-BASED NANOSTRUCTURES BY CHEMICAL VAPOUR GROWTH ON SILICON WAFER AND FROM PYROLYSIS OF OIL PALM FIBRES

by

CHIEW YI LING

Thesis submitted in fulfillment of the requirements for the degree of Master of Science

MAY 2012

ACKNOWLEDGEMENT

First and foremost, I would like to express my heartfelt thanks and gratitude to my supervisor, Assoc. Prof. Ir. Dr. Cheong Kuan Yew for his constant guidance and advices. With his help and support, I have improved myself in more than one ways besides being able to finish the dissertation. I would also like to thank Professor Ahmad Fauzi bin Mohd Noor, the Dean of the School of Materials and Mineral Resources Engineering.

I am also very thankful to Universiti Sains Malaysia for providing me financial supports from Universiti Sains Malaysia Research University Grant and USM RU-PRGS grant (1001/PBAHAN/8033004).

In addition, I am grateful to all the staffs and technicians, especially Mr. Shahrul, Mdm. Fong, Mr. Suhaimi, Mr. Rashid, Mr. Khairi and Mr. Azrul for their technical support. Their cooperation and efforts will always be appreciated.

And last but not least, I would like to thank my family and friends for their constant support. It had been challenging in the process of completing this dissertation and without their constant support and advice, I would not have successfully gone through this period. And thus, I am thoroughly grateful for having them by my side.

CHIEW YI LING
2012
Universiti Sains Malaysia (USM).

TABLE OF CONTENTS

ACKNOWLEDGEMENT ii

TABLE OF CONTENTS iii

LIST OF TABLES vii

LIST OF FIGURES vii

LIST OF ABBREVIATIONS xiii

LIST OF PUBLICATIONS xiv

ABSTRAK xv

ABSTRACT xvii

CHAPTER 1 INTRODUCTION 1

1.1 Introduction 1

1.2 Problem Statement 3

1.3 Research Objectives 5

1.4 Scope of Research 5

CHAPTER 2 LITERATURE REVIEW 7

2.1 Introduction 7

2.2 Si-Based Nanostructures 7

2.2.1 Nanostructures 7

2.2.2 Silicon Carbide (SiC) 8

2.2.3 Silica (SiO_2) 13

2.2.4 Synthesis of Si-Based Nanostructures 14

2.3 Direct Growth of Si-Based Nanostructures on Si Substrate 16

2.3.1 Effect of Starting Materials 16

2.3.1.1 Si source 16

2.3.1.2 Carbon Source 18

2.3.2 Effect of Growth Temperature 20

2.3.3 Effect of Catalyst 21
2.3.4 Effect of Furnace Atmosphere 22
2.4 Pyrolysis of Biomass 25
2.4.1 Biomass 25
2.4.1.1 Oil Palm Empty Fruit Bunch Fibres 26
2.4.1.2 Rice Husk 27
2.4.2 Formation of SiC Nanostructures from Pyrolysis of Biomass 28
2.4.2.1 Kinetics and Processes 29
2.4.2.2 Effect of Starting Materials 33
2.4.2.3 Effect of Acid Treatment 35
2.4.2.4 Effect of Temperature 38
2.4.2.5 Effect of Holding Time 40
2.4.2.6 Effect of Catalyst 41
2.4.2.7 Effect of Furnace Atmosphere 45
CHAPTER 3 MATERIALS AND METHODOLOGY 47
3.1 Introduction 47
3.2 Chemical Vapour Growth (CVG) on Si Wafers 49
3.2.1 Chemicals and Reagents 50
3.2.2 Wafer Preparation 50
3.2.3 Thermal Oxidation of Silicon Wafer 52
3.2.4 Growth of Nanostructures in Vacuum Sintering Furnace 53
3.3 Pyrolysis of Oil Palm Empty Fruit Bunch Fibres 55
3.3.1 Chemicals and Reagents 57
3.3.2 Preparation of Oil Palm Empty Fruit Bunch Fibres 57
3.3.2.1 Cleaning of Oil Palm Empty Fruit Bunch Fibres 57
3.3.2.2 Hydrochloric Acid (HCl) Treatment of Empty Fruit Bunch Fibres 58

3.3.2.3 Cutting of Acid-treated Oil Palm Empty Fruit Bunch (TOP) fibres 58
3.3.3 Preparation of Si source for Pyrolysis 59
3.3.3.1 Rice Husk Ash (RHA) 59
3.3.3.2 Tetraethyl orthosilicate (TEOS) 59
3.3.4 Growth of Nanostructures in Horizontal Tube Furnace 60
3.3.5 Decarbonization 61
3.3.6 Hydrofluoric Acid (HF) Treatment 61
3.4 Characterization 62
3.4.1 X-ray Fluorescence (XRF) 63
3.4.2 Carbon/Hydrogen/Nitrogen/Sulphur Elemental Analyzer (CHNS) 63
3.4.3 Field-Emission Scanning Electron Microscope (FESEM) 64
3.4.4 Energy-Filtered Transmission Electron Microscope (EFTEM) 65
3.4.5 X-ray Diffraction (XRD) 66
3.4.6 Fourier Transform Infrared Spectrophotometer (FTIR) 66
CHAPTER 4 RESULTS AND DISCUSSION 68
4.1 Introduction 68
4.2 Chemical Vapour Growth (CVG) on Si Wafers 69
4.2.1 Effect of Oxidation Time 69
4.2.2 Effect of Soaking Time in Vacuum Sintering Furnace 73
4.2.3 Effect of Activated Carbon Powder Amount 77
4.2.4 Growth Mechanism 86
4.2.4.1 Formation of SiC Nanorods and SiC Nanocolumns 89
4.2.4.2 Formation of SiC/SiO_2 core-shell clusters, nanowires, nanowebs and nanocables 91
4.3 Pyrolysis of Oil Palm Fibres 97
4.3.1 RHA as Silicon Source 97
4.3.1.1 Effect of RHA Amount 97

4.3.1.2 Effect of Growth Temperature 105

4.3.1.3 Growth Mechanism 110

4.3.2 TEOS as Silicon Source 114

4.3.2.1 Effect of TEOS Concentration 114

4.3.2.2 Effect of Pyrolysis Temperature 123

4.3.2.3 Growth Mechanism 127

4.3.3 Comparison between RHA and TEOS as Silicon Source 130

4.4 Summary of Synthesis Methods between CVG on Si Wafers and Pyrolysis of Oil Palm Fibres 132

CHAPTER 5 CONCLUSION 134

5.1 Conclusion 134

5.2 Recommendations for Future Work 137

REFERENCES 138

APPENDICES 152

LIST OF TABLES

Table 2.1:	Properties for different polytypes of SiC and SiC nanowires at room temperature.	10
Table 2.2:	Properties of SiO_2 nanowires at room temperature.	14
Table 2.3:	Comparison of several synthesis methods of Si-based nanostructures (Zhou et al., 2008).	15
Table 2.4:	Percentage of SiO_2 in different types of agricultural wastes.	28
Table 2.5:	Dependency of pyrolysis reaction on temperature (Krishnarao and Mahajan, 1996a, Chandrasekhar et al., 2005).	38
Table 2.6:	List of catalyst incorporated in rice husk during growth of SiC.	42
Table 3.1:	Specifications of the chemicals and reagents used in CVG on Si wafers.	50
Table 3.2:	Experimental parameters used in CVG on Si wafers.	55
Table 3.3:	Specifications of the chemicals and reagents used in pyrolysis of oil palm fibres.	57
Table 3.4:	Experimental parameters used in pyrolysis of TOP fibres.	61
Table 4.1:	Summary of nanostructures formed on Si wafer depending on the amount of ACP and the location on Si wafer.	78
Table 4.2:	Chemical compositions of OP, TOP and RHA.	97
Table 4.3:	Absorption bands in FTIR spectra and their assignments.	100
Table 4.4:	Chemical compositions of OP, TOP, 0.1TEOS, 0.5TEOS and 1.0TEOS.	115
Table 4.5:	Absorption bands in FTIR spectra and their assignments.	120
Table 4.6:	Comparison of the nanostructures formed using different Si source of RHA and TEOS.	130
Table 4.7:	Comparison of synthesis methods between CVG on Si wafers and pyrolysis of oil palm fibres.	132

LIST OF FIGURES

Figure 2.1:	Tetrahedral bonding of a C atom with its four nearest Si atoms.	9
Figure 2.2:	Stacking sequence of double layers of 3C, 4H, 6H and 15R-SiC (Sudarshan, 2006).	10
Figure 2.3:	Tetrahedral bonding of a Si atom with its four nearest O atoms.	13
Figure 2.4:	Plot of SiC yield against temperature for fine/coarse samples and loose/compact samples (Panigrahi et al., 2001).	34
Figure 2.5:	XRD patterns of (a) raw rice husk samples and (b) acid-treated rice husk samples under different temperatures (Krishnarao et al., 2001).	37
Figure 2.6:	XRD patterns of pyrolyzed raw rice husk samples at atmospheric pressure for different temperatures (Krishnarao and Mahajan, 1996a).	39
Figure 2.7:	Evolution of SiC yield as a function of holding time at 1400°C: (O) 1% Fe; (□) 5% Fe; (Δ) uncatalysed (Narciso-Romero and Rodriguez-Reinoso, 1996).	40
Figure 2.8:	XRD diffractograms of samples prepared at 1400°C (5 hour reaction) catalyzed by iron, cobalt and nickel (5% loading) (Narciso-Romero and Rodriguez-Reinoso, 1996).	42
Figure 3.1:	Overview of the research approaches in obtaining Si-based nanostructures.	48
Figure 3.2:	Flow chart of the experimental methodologies in CVG.	49
Figure 3.3:	Heating profile for thermal oxidation in horizontal tube furnace.	53
Figure 3.4:	Experimental setup in the vacuum sintering furnace.	54
Figure 3.5:	Heating profile in vacuum sintering furnace.	55
Figure 3.6:	Flow chart of the experimental methodologies in pyrolysis of oil palm fibres.	56
Figure 3.7:	Experimental setup in the horizontal tube furnace.	60
Figure 3.8:	Heating profile in horizontal tube furnace.	61
Figure 4.1:	A representative FESEM image of the oxidized silicon wafer at an oxidation time of 12 mins.	69

Figure 4.2: FESEM images of the nanorods and nanocolumns formed at the centre and the sides of silicon wafer when heated at 1300°C for 1 hour under different oxidation time of 1 min, 2 mins, 8 mins and 12 mins. 70

Figure 4.3: EDS results of the nanorods at the centre of silicon wafer under different oxidation times of (a) 1 min, (b) 2 mins, (c) 8 mins and (d) 12 mins. 71

Figure 4.4: EDS results of the nanorods at the side of silicon wafer under different oxidation times of (a) 1 min, (b) 2 mins, (c) 8 mins and (d) 12 mins. 71

Figure 4.5: An EFTEM image of the nanostructures formed on a silicon wafer at the oxidation time of 2 mins and scrapped from the centre of wafer surface. 72

Figure 4.6: FESEM micrographs of nanostructures formed at the centre of Si wafer under different soaking time of (a) 1 hour (Inset showing higher magnification micrograph of the nanostructures) and (b) 2 hours. 74

Figure 4.7: EDS results of the grains formed at the centre of Si wafer under a soaking time of 2 hours. 74

Figure 4.8: (a) and (b) shows the FESEM micrographs of nanocolumns formed at the side of Si wafer under a soaking time of 1 hour while (c) and (d) shows the FESEM micrographs of nanowires and nanowebs formed at the side of wafer under a soaking time of 2 hours. 75

Figure 4.9: EFTEM images of (a) nanorods or nanocolumns formed under soaking time of 1 hour and (b) core-shell nanowires formed under soaking time of 2 hours. 76

Figure 4.10: ESI results showing composition of nanowires formed under soaking time of 2 hours. 76

Figure 4.11: Location of nanostructures formed on the SiO_2/Si wafer. 77

Figure 4.12: FESEM images of nanostructures formed at the centre under different ACP amount of (a) 0 g, (b) 0.5 g, (c) 1.0 g and (d) 1.5 g. 79

Figure 4.13: EDS results of the (a) unetched Si wafer surface and (b) voids formed on Si wafer at the centre. 79

Figure 4.14: FESEM images of nanostructures formed at the border under different ACP amount of (a) 0 g, (b) 0.5 g, (c) 1.0 g and (d) 1.5 g. 80

Figure 4.15: EDS results of the nanowebs at the borders at two different locations showing (a) only Si and O and (b) Si, O and C. 80

Figure 4.16: EFTEM images of nanostructures formed at the border under different ACP amount of (a) 0 g, (b) 0.5 g, (c) 1.0 g and (d) 1.5 g. 81

Figure 4.17: FESEM images of nanostructures formed at the side under different ACP amount of (a) 0 g, (b) 0.5 g, (c) 1.0 g and (d) 1.5 g (Inset showing higher magnification of the nanowire cluster formed in 1.5ACP). 82

Figure 4.18: EDS results of (a) and (b) randomly oriented nanowires when exposed to 0 g, 0.5 g and 1.0 g ACP as well as (c) and (d) the nanowire clusters formed when exposed to 1.5 g ACP at the sides of Si wafer. 83

Figure 4.19: EFTEM images of nanostructures formed at the side under different ACP amount of (a) 0 g, (b) 0.5 g, (c) 1.0 g and (d) 1.5 g (Circled shows the presence of stacking faults). 84

Figure 4.20: (a) ESI results of the core-shell nanowires at the side of wafer, (b) ESI results of the nanowebs at the border and (c) XRD spectrum of the samples. 85

Figure 4.21: Aerodynamic effects inside the crucible during heating in furnace. 89

Figure 4.22: Growth mechanisms of nanorods and nanocolumns at the centre and side of silicon wafer. 91

Figure 4.23: Growth mechanisms of clusters at the centre of silicon wafer at a soaking time of 2 hours. 92

Figure 4.24: Growth mechanisms of nanowires, nanowebs and nanocables at the border of silicon wafer at a soaking time of 2 hours. 93

Figure 4.25: Influence of Venturi effect on the flow of reactant species as they passed through the gap at the border. 93

Figure 4.26: Formation of SiC/SiO_2 nanocable, nanoweb and amorphous SiO_2 branch through self-organization and oxide growth. 95

Figure 4.27: (a) Influence of Venturi effect on the flow of reactant species as it exited the gap at the side of wafer. (b) Growth mechanisms of nanowires at the side of silicon wafer at a soaking time of 2 hours. 96

Figure 4.28: Appearance of the pyrolyzed TOP/RHA mixtures with (a)-(d) showing the mixtures after pyrolysis and (e)-(h) showing the mixtures after decarbonization for 0.2RHA, 0.4RHA, 0.6RHA and 0.8RHA, respectively. 98

Figure 4.29: FESEM micrographs of pyrolyzed TOP/RHA mixtures at different amounts of RHA of (a) 20%, (b) 40%, (c) 60% and (d) 80%. Insets of (a)-(c) show the higher magnification micrographs of the pyrolyzed TOP/RHA mixtures. (e) shows the nanocones formed in 0.8RHA. Circled shows the spherical metal catalyst cap on the tips of the nanocones. 100

Figure 4.30: FTIR spectra of (a) the raw materials and the TOP/RHA mixtures after the process of (b) pyrolysis, (c) decarbonization and (d) HF treatment under different RHA amounts. 103

Figure 4.31: EFTEM images of the nanostructures formed in (a) 0.2RHA, (b) 0.4RHA, (c) 0.6RHA and (d) 0.8RHA. (e) and (f) show the composition of nanowires and nanoparticles determined by ESI. (g) shows the diameter distribution of the nanostructures formed under different RHA amounts. 104

Figure 4.32: A representative XRD spectrum of the nanowires formed from TOP/RHA mixture after HF treatment. 105

Figure 4.33: Appearance of the pyrolyzed TOP/RHA mixtures with (a)-(d) showing the mixtures after pyrolysis and (e)-(h) showing the mixtures after decarbonization at pyrolysis temperatures of 1250°C, 1300°C, 1350°C and 1400°C, respectively. 106

Figure 4.34: FESEM micrographs of pyrolyzed TOP/RHA mixture fixed at 0.4RHA at different pyrolysis temperatures of (a) 1250°C, (b) 1300°C, (c) 1350°C and (d) 1400°C. Insets show the higher magnification micrographs of the pyrolyzed TOP/RHA mixtures. 107

Figure 4.35: FTIR spectra of (a) the raw materials and the TOP/RHA mixtures fixed at 0.4RHA after the process of (b) pyrolysis, (c) decarbonization and (d) HF treatment under different pyrolysis temperatures. 108

Figure 4.36: EFTEM images of the nanostructures formed under different pyrolysis temperatures of (a) 1250°C, (b) 1300°C, (c) 1350°C and (d) 1400°C. (e) shows the diameter distribution of the nanostructures formed under different pyrolysis temperatures. 109

Figure 4.37: EDS results of the nanostructures formed. 111

Figure 4.38: Growth mechanisms of the nanowires and nanocones. 114

Figure 4.39: FESEM micrographs of TOP fibres (a) before TEOS infiltration and after TEOS infiltration with (b) 10 % TEOS, (c) 50 % TEOS and (d) 100 % TEOS. 116

Figure 4.40: Appearance of the pyrolyzed TEOS-filled TOP samples with (a)-(c) showing samples after pyrolysis and (d)-(f) showing samples after decarbonization for 0.1TEOS, 0.5TEOS and 1.0TEOS, respectively. 117

Figure 4.41: FESEM micrographs of pyrolyzed TEOS-filled TOP samples at different TEOS concentrations of (a) 0.1TEOS, (b) 0.5TEOS and (c) 1.0TEOS at low magnification and (d)-(f) along with the insets show higher magnification micrographs of the nanowires at concentrations of 0.1TEOS, 0.5TEOS and 1.0TEOS, respectively. 118

Figure 4.42: FTIR spectra of (a) TOP and after each process of (b) pyrolysis, (c) decarbonisation and (d) HF treatment under different TEOS concentrations. 120

Figure 4.43: EFTEM images of the nanowires formed in (a) 0.1TEOS, (b) 0.5TEOS and (c) 1.0TEOS. (d) shows the composition of nanowires determined by ESI and (e) shows the diameter distribution of the nanowires at different TEOS concentrations. 122

Figure 4.44: A representative XRD spectrum of the nanowires after HF treatment. 123

Figure 4.45: Appearance of the pyrolyzed TEOS-filled TOP samples fixed at 10% TEOS with (a)-(d) showing the samples after pyrolysis and (e)-(h) showing the samples after decarbonisation at pyrolysis temperatures of 1250°C, 1300°C, 1350°C and 1400°C, respectively. 124

Figure 4.46: FESEM micrographs of pyrolyzed TEOS-filled TOP samples fixed at 10% TEOS at different pyrolysis temperatures of (a) 1250°C, (b) 1300°C, (c) 1350°C and (d) 1400°C. Insets show the higher magnification micrographs of the pyrolyzed TEOS-filled TOP samples. 125

Figure 4.47: FTIR spectra of (a) TOP and the samples after the process of (b) pyrolysis, (c) decarbonisation and (d) HF treatment under different pyrolysis temperatures fixed at 10% TEOS. 126

Figure 4.48: EFTEM images of the nanostructures formed under different pyrolysis temperatures of (a) 1250°C, (b) 1300°C, (c) 1350°C and (d) 1400°C. (e) shows the composition of the nanowires and particles using ESI and (f) shows the diameter distribution of the nanostructures formed under different pyrolysis temperatures. 127

Figure 4.49: (a) FESEM micrograph showing the origin of an individual nanowire growing from a cluster and the corresponding EDS results of the cluster at the base of nanowire in (b). 128

LIST OF ABBREVIATIONS

0D	Zero-dimensional
1D	One-dimensional
2D	Two-dimensional
ACP	Activated carbon powder
CHNS	Carbon/Hydrogen/Nitrogen/Sulphur
CVD	Chemical vapor deposition
CVG	Chemical vapor growth
EDS	Energy dispersive X-ray spectrometer
EFTEM	Energy-filtered transmission electron microscope
ESI	Electron spectroscopic imaging
FESEM	Field-emission electron microscope
FTIR	Fourier transform infrared spectrophotometer
HMDS	Hexamethyldisilane
LOI	Loss on ignition
NEMS	Nanoelectromechanical systems
OAG	Oxide-assisted growth
OP	Oil palm empty fruit bunch fibres
RHA	Rice husk ash
SLS	Solid-liquid-solid
TEOS	Tetraethyl orthosilicate
TOP	Acid-treated fibres
VLS	Vapor-liquid-solid
VS	Vapor-solid
XRD	X-ray diffraction
XRF	X-ray fluorescence

LIST OF PUBLICATIONS

Chiew, Y. L. and Cheong, K. Y. (2012) Growth of SiC Nanowires and Nanocones Using Mixture of Oil Palm Fibres and Rice Husk Ash. *Journal of Materials Science*, Article in Press (DOI: 10.1007/s10853-012-6438-7).

Chiew, Y. L. and Cheong, K. Y. (2012) Synthesis of SiC Nanostructures through Chemical Vapor Growth Route. *International Journal Materialwissenschaft Und Werkstofftechnik (Materials Science and Engineering Technology)*, 43, No. 5, 1-4. (doi.: 10.1002/mawer.201200974).

Chiew, Y. L. and Cheong, K. Y. (2011) A review on the synthesis of SiC nanostructures from plant-based biomasses. *Materials Science and Engineering B*, 176, 951-964. (doi.: 10.1016/j.msed.2011.05.037).

Chiew, Y. L. and Cheong, K. Y. (2011) Synthesis of SiC Nanostructure Through Chemical Vapor Growth Route. *5th International Conference on Advanced Computational Engineering and Experimenting (ACE-X 2011)*, 3 – 6 July 2011, Algarve, Portugal, pp. 170 - 171.

SINTESIS STRUKTUR-STRUKTUR NANO BERASASKAN SILIKON MELALUI PERTUMBUHAN SECARA PEMERUAPAN KIMIA ATAS WAFER SILIKON DAN PIROLISIS GENTIAN KELAPA SAWIT

ABSTRAK

Struktur-struktur nano berasaskan silikon disintesis dengan menggunakan dua cara, iaitu pertumbuhan secara pemeruapan kimia (CVG) atas wafer silikon dan pirolisis gentian kelapa sawit. Dalam CVG, nanorod dan nanotiang SiC serta nanowayar, nanokabel dan nanosarang SiC/SiO_2 dihasilkan dengan memanaskan wafer silikon dan serbuk karbon aktif (ACP) di dalam vakum/argon pada 1300°C. Masa pengoksidaan, masa perendaman dan kuantiti ACP mempengaruhi hasil pertumbuhan. Nanorod dan nanotiang SiC dihasilkan pada masa perendaman 1 jam, di mana diameter dan hasil pertumbuhan bertambah apabila masa pengoksidaan naik daripada 1 kepada 12 minit. Strukturnya tukar kepada kelompok, nanowayar, nanokabel dan nanosarang SiC/SiO_2 bersama dengan nanowayar SiO_2 di lokasi berbeza atas wafer pada masa perendaman 2 jam. Diameternya susut apabila kuantiti ACP ditingkatkan. Pembentukan hasil berlainan ini adalah disebabkan oleh kesan aerodinamik kerana perbezaan tekanan di dalam dan luar mangkuk pijar. Pertumbuhan struktur nano SiC ini adalah melalui mekanisma wap-pepejal. Dalam pirolisis gentian kelapa sawit, nanowayar dan nanokon SiC dihasilkan dengan memanaskan gentian kelapa sawit dengan abu sekam padi (RHA) atau tetraetil orthosilikat (TEOS) sebagai sumber karbon dan silikon di bawah atmosfera argon. Sampel TEOS menghasilkan lebih banyak nanowayar. Kuantiti sumber silikon dan suhu pirolisis mempengaruhi hasil pertumbuhan. Apabila RHA digunakan dan kuantitinya ditingkatkan kepada 80%, strukturnya tukar daripada nanowayar kepada nanokon SiC. Jadi, 40% RHA merupakan kuantiti ideal untuk mendapatkan nanowayar dalam kuantiti maximum dan kekotoran minimum.

Peningkatan suhu meningkatkan hasil pertumbuhan. Apabila TEOS digunakan, hanya nanowayar SiC dihasilkan dan peningkatan kepekatan TEOS menyebabkan hasil pertumbuhan nanowayar meningkat tetapi hanya setakat kepekatan tertentu kerana pada kepekatan tinggi, TEOS mempunyai kebendaliran rendah. Jadi, 10% TEOS merupakan kepekatan ideal. Apabila suhu pembakaran ditingkatkan, diameternya turun. Penurunan diameter adalah disebabkan oleh kadar penyahjerapan atom yang lebih tinggi pada suhu tinggi. Pertumbuhan nanowayar SiC adalah melalui mekanisma wap-pepejal dengan mekanisma wap-cecair-pepejal sebagai mekanisma sekunder yang didorongi oleh sisa logam. Pertumbuhan nanokon adalah melalui mekanisma wap-pepejal yang didorongi oleh titisan besar logam.

SYNTHESIS OF SILICON-BASED NANOSTRUCTURES BY CHEMICAL VAPOUR GROWTH ON SILICON WAFER AND FROM PYROLYSIS OF OIL PALM FIBRES

ABSTRACT

Silicon-based nanostructures were successfully synthesized from two different routes of chemical vapour growth (CVG) on silicon wafers and pyrolysis of oil palm fibres. In CVG, SiC nanorods, SiC nanocolumns as well as SiC/SiO_2 core-shell nanowires, nanocables and nanowebs were produced by heating only Si wafers and activated carbon powder (ACP) under vacuum/argon at 1300°C. The oxidation time, soaking time and amount of ACP influenced the morphologies of nanostructures. SiC nanorods and nanocolumns were formed at soaking time of 1 hour, with increasing diameter and yield when oxidation time was raised from 1 to 12 minutes. The structure then changed to SiC/SiO_2 core-shell clusters, nanowires, nanocables and nanowebs along with some SiO_x nanowires when soaking time was 2 hours, at different locations on silicon wafers that decreased in diameter with increasing amount of ACP. The different nanostructures were a result of aerodynamic effects in the crucible due to pressure difference inside and outside the crucible. The growth of these nanostructures was under vapour-solid mechanism. In pyrolysis of oil palm fibres, SiC nanowires and nanocones were produced by heating oil palm empty fruit bunch fibres and rice husk ash (RHA) or tetraethyl orthosilicate (TEOS) as carbon and silicon sources, respectively, under argon atmosphere, though TEOS-impregnated samples showed higher yield of nanowires. The amount of Si sources and pyrolysis temperature influenced the products formed. When RHA was used and the amount was increased to 80%, structure changed from SiC nanowires to nanocones but overall, 40% RHA was the ideal amount in growing nanowires with maximum yield and least impurities.

When pyrolysis temperature was raised, there was an increase in the yield. When TEOS was used, only SiC nanowires were formed and an increase in TEOS concentration led to an increase in the yield but only to a certain extent due to lower fluidity of TEOS at higher concentrations. Thus, 10% TEOS was the ideal concentration. When pyrolysis temperature was raised, a decrease in diameter was observed in TEOS samples. The diameter drop was an effect of higher atom desorption rate at higher temperatures. The growth of nanowires was attributed to combination of solid-state and vapour-solid mechanism, with secondary mechanism of vapour-liquid-solid mechanism induced by trace metals. Whereas the growth of nanocones was attributed to vapour-liquid-solid mechanism induced by larger metallic droplets.

CHAPTER 1

INTRODUCTION

1.1 Introduction

Nanostructures have been gaining worldwide interest due to their small sizes that enable higher functionalities in a given space and their peculiar and fascinating properties, which make them applicable in mesoscopic research, development of nanodevices and potential applications of large surface area structures (Xia et al., 2003). These nanostructures are particularly interesting especially one-dimensional (1D) structures, such as nanotubes, nanowires and nanorods that have garnered the attentions of researchers and led to the development of various materials in nanoscale. Nanowires, which are one of the 1D nanostructures, have been used as versatile building blocks in the miniaturization of electronic and optoelectronic devices (Li et al., 2006). Various materials have been synthesized in the form of nanowires, such as silicon, germanium, gallium nitride, gallium arsenide and silicon carbide (Spanier, 2006).

Silicon-based nanostructures, which include SiC and SiO_2 nanostructures, have become one of the focuses of these intensive researches because of their unique properties. Silicon carbide (SiC) nanostructures exhibit excellent semiconducting, mechanical, thermal, chemical and optical properties that make them applicable in many areas especially in high temperature, high frequency and high power applications (Shen et al., 2003), such as nanoelectronics, nanooptics, nanosensors (Wei et al., 2002) and nanoelectromechanical systems (NEMS) (Choi et al., 2004). Presence of oxide layer surrounding the SiC nanostructures, constituting the SiC/SiO_2 core-shell nanostructures, was also reported to enhance the photoluminescence properties of SiC (Feng et al.,

2003, Cai et al., 2005, Liu and Yao, 2005, Kim et al., 2009) as well as the mechanical strength of composite by improving the interface bonding intensity of SiC in rubber (Meng et al., 2007), while being able to maintain the intrinsic properties of SiC. The distinctive semiconducting and optical properties of silica (SiO_2) nanostructures also make them potential candidates in nanooptics and nanosensors applications (Pan et al., 2001). Furthermore, these Si-based nanostructures are known to exhibit good biocompatibility, suggesting possible applications in biomedical field (Fan et al., 2006).

As a result, several methods have been developed to synthesize these Si-based nanostructures, with some of the common ones being laser ablation (Yu et al., 1998, Seeger et al., 2000), sol–gel (Liang et al., 2000b, Meng et al., 2000), thermal evaporation (Wei et al., 2006), carbothermal reduction (Shi et al., 2000b, Wu et al., 2001), rapid thermal annealing (Lai et al., 2008), chemical vapour deposition (CVD) (Zhou et al., 1999, Mamails et al., 2004, Zhang et al., 2006) and thermal oxidation route (Hu et al., 2003). Here, two routes are used to synthesize these Si-based nanostructures, namely chemical vapour growth (CVG) growth on Si wafers and pyrolysis of oil palm fibres, where one involves the growth of nanostructures on a substrate and the other involves the growth of stand-alone nanostructures. The CVG growth on Si wafers route refers to the growth of the nanostructures directly on the Si wafers by heating only Si wafers and C powders without the assistance of any metallic catalyst. This route was able to produce different nanostructures of SiC/SiO_2 and SiO_2 in the form of clusters, nanowires, nanorods, nanocolumns, nanocables and nanowebs. For the case of pyrolysis of oil palm fibres, SiC nanowires and nanocones were produced by simply pyrolyzing the oil palm empty fruit bunch fibres mixed with rice husk ash or tetraethyl orthosilicate (TEOS), with the oil palm fibres acting as carbon source and rice husk ash or TEOS acting as silicon source. Although oil palm fibres

contain inherent SiO_2, additional silicon source is necessary because a control experiment performed by pyrolyzing the oil palm fibres alone showed that no nanostructures were formed.

1.2 Problem Statement

Although a variety of methods have been developed for the synthesis of nanostructures, the advancement in the field of nanotechnology is hindered due to the difficulties arising from the aspect of inability to control the dimensions, morphology, phase purity and the chemical composition of the nanostructures.

In the CVG route, similar direct growth routes had been used to synthesize these Si-based nanostructures though the reaction conditions differed in terms of starting materials, growth temperature and addition of catalyst (Li et al., 2002, Ryu et al., 2004, Baek et al., 2006, Du et al., 2007, Niu and Wang, 2007b, Park et al., 2007, Wang et al., 2007, Jeong et al., 2008, Al-Ruqeishi et al., 2010, Liao et al., 2012). In these reports, most used bare Si wafers to grow the nanostructures (Ryu et al., 2004, Niu and Wang, 2007a, Wang et al., 2007, Al-Ruqeishi et al., 2010). However, it was reported that the presence of a thin oxide layer was found to enhance the growth of Si-based nanostructures (Li et al., 2002, Park et al., 2007, Jeong et al., 2008). Some also reported the use of metallic catalysts in these methods to induce the growth of nanostructures (Li et al., 2002, Ryu et al., 2004, Baek et al., 2006, Niu and Wang, 2007a, Wang et al., 2007, Attolini et al., 2008, Lopez-Camacho et al., 2008, Kim et al., 2009, Niu and Wang, 2009, Al-Ruqeishi et al., 2010, Liao et al., 2012). Although the use of metallic catalysts helped to reduce the growth temperature and improve the yield, it limited the applications of the nanostructures formed because the metallic catalysts

acted as impurities that could degrade the properties of the devices formed (Yao et al., 2005, Colli et al., 2006). Hence, a simple, catalyst-free method is proposed in this study by heating directly pre-oxidized silicon wafers and activated carbon powder to grow the Si-based nanostructures.

As for pyrolysis of oil palm fibres, the use of these plant-based biomasses to produce the nanostructures offers an economical and environmental friendly approach in disposing these wastes while being able to produce something useful. Similar routes had been used in producing the nanostructures by pyrolyzing either rice husk (Lee and Cutler, 1975), coconut shell (Selvam et al., 1997, Nair, 1999), sugarcane leaf with rice straw (Patel and Kumari, 1990), bean-curd refuse (Motojima et al., 1995) or cotton fibre (Weaver, 1989, Krishnarao and Mahajan, 1996b) but there were no reports on the growth of Si-based nanostructures using oil palm fibres. Every year, Malaysia produces a substantial amount of agricultural wastes, around 20 million tonnes of oil palm empty fruit bunch fibres (ASEAN Secretariat, 2009) and 8.4×10^5 tonnes of rice husks (Isa et al., 2009). Oil palm fibres have been reported to contain high carbon content and low ash content that indicate that the carbon materials from oil palm fibres are of high purity and this makes them a suitable choice of carbon in producing SiC nanowires (Lua and Guo, 1998). Whereas rice husks are suitable sources of silicon since they contain unusually high percentages of amorphous silica at around 15 – 28% (Lee and Cutler, 1975, Sharma et al., 1984, Sun and Gong, 2001, Chandrasekhar et al., 2005).

1.3 Research Objectives

The objectives of these studies based on the two different synthesis routes are:-

1. CVG Growth on Si Wafers
    a. To investigate the effects of oxidation time (1 min, 2 mins, 8 mins and 12 mins), soaking time (1 and 2 hours) and amount of activated carbon powder (0 g, 0.5 g, 1.0 g and 1.5 g) on the growth of Si-based nanostructures via CVG method.
    b. To establish the growth mechanisms of the nanostructures.
2. Pyrolysis of Oil Palm Fibres
    a. To investigate the effects of the amount of rice husk ash (20, 40, 60 and 80%), TEOS concentration (10, 50 and 100%), and growth temperature (1250°C – 1400°C) on the growth of SiC nanostructures by using mixture of oil palm fibres and rice husk ash or TEOS-impregnated oil palm fibres under pyrolysis method.
    b. To establish the growth mechanisms of the nanostructures.

1.4 Scope of Research

In this study, Si-based nanostructures were synthesized through two routes of CVG growth on Si wafers and pyrolysis of oil palm fibres.

In the CVG direct growth on Si wafers, this was conducted using a modified CVD approach in a vacuum sintering furnace. This synthesis method involved a silicon wafer first subjected to thermal oxidation for a certain period (1 min, 2 mins, 8 mins and 12 mins) to introduce a thin oxide layer, followed by heating under Ar flow at growth temperature of 1300°C for 1 to 2 hours while exposed to different amounts of

activated carbon powder (0 g, 0.5 g, 1.0 g and 1.5 g). The characterization techniques involved were field-emission scanning electron microscope (FESEM, LEO GEMINI) equipped with an energy dispersive X-ray spectrometer (EDS, ZEISS SUPRA^{TM} 35VP), an energy-filtered transmission electron microscope (EFTEM, ZEISS LIBRA 120) equipped with an electron spectroscopic imaging (ESI) and X-ray diffraction (XRD, Bruker D8).

In the pyrolysis of oil palm fibres, this synthesis method involved pyrolyzing mixture of acid-treated oil palm fibres and rice husk ash or TEOS-impregnated oil palm fibres in a horizontal tube furnace at growth temperatures of 1250 - 1400°C for 1 hour using different amounts of rice husk ash (20%, 40%, 60% and 80%) or TEOS concentration (10%, 50% and 100%) under argon atmosphere. The characterization methods involved X-ray fluorescence (XRF, Casio), a Carbon/Hydrogen/Nitrogen/Sulphur (CHNS) elemental analyser (Perkin Elmer 2400), a FESEM (ZEISS LIBRA 120) equipped with EDS (ZEISS SUPRA^{TM} 35VP),, an EFTEM (ZEISS LIBRA 120) equipped with ESI, XRD (Bruker D8) and fourier transform infrared spectrophotometer (FTIR, Perkin-Elmer System 2000).

CHAPTER 2

LITERATURE REVIEW

2.1 Introduction

In this chapter, a brief background on the structures, properties and general synthesis routes of Si-based nanostructures especially for silicon carbide (SiC) and silica (SiO_2) will be described. Since two synthesis routes of direct growth on Si substrates and pyrolysis of biomass have been used, previous studies similar to these methods will also be reviewed in terms of the processes and the effects of the different parameters in the following sections.

2.2 Si-Based Nanostructures

2.2.1 Nanostructures

A nanostructured material can be defined as a material whose composition is modulated over nanometer range from 1 nm to 100 nm. They can be classified into zero, one and two dimensionalities based on geometrical shapes (Cao, 2004a).

Zero-dimensional (0D) nanostructures are materials in which all three dimensions are in nanometer scale such as nanoparticles, nanospheres and nanoclusters and they have been widely studied for their potential applications as multifunctional nanoparticle probe (Cao, 2004a). One-dimensional (1D) nanostructures are materials in which two of their dimensions are in nanometer scale. Variety of names has been given to 1D nanostructures depending on their shapes and sizes such as whiskers, fibres, nanorods and nanowires. Nanowires and nanorods are actually similar to whiskers and fibres

respectively. They only differ in terms of the diameters of the product, with the diameters of the nanowires and nanorods in the range of 1 nm to 100 nm whereas the diameters of the whiskers and fibres to be in the range of 100 nm to 10000 nm (Weaver, 1989, Narciso-Romero and Rodriguez-Reinoso, 1996). Nanowires have aspect ratio of more than 10 whereas nanorods have aspect ratio of less than 10 (Narciso-Romero and Rodriguez-Reinoso, 1996). 1D nanostructures are known to exhibit quantum confinement effect like 0D nanostructures. The quantum confinement effect could be observed when the diameter of material is less than the Bohr radius of that material (Bae et al., 2003). So, for the 1D nanostructures, the charge carriers can only travel in one direction along the wire and thus, make them useful as interconnects and critical devices in nano-electronic and nano-optoelectronic applications (Cao, 2004a). Two-dimensional (2D) nanostructures are materials having nanometer dimension perpendicular to the layer plane such as thin film and nanoporous materials. The charge carriers in these 2D nanostructures are limited to the direction perpendicular to the layer and can move freely in the layer plane. These 2D nanostructures especially nanoporous materials have been studied for their applications in biosensors, nanophotonics and nano-electronic applications.

2.2.2 Silicon Carbide (SiC)

SiC was first discovered accidentally when a Swedish scientist, Jöhn Jacob Berzelius was trying to synthesize diamond in 1824 (Zimmermann, 19 December 2000). It was then largely manufactured when Cowless (1885) and Acheson (1892) found that the hard and stable compound was suitable for grinding and cutting purposes and Acheson

developed an industrial method which involved carbothermal reduction of silica sand with green petroleum coke at temperature of 2400°C (Sudarshan, 2006).

SiC is a covalently-bonded IV-IV compound with alternating layers of silicon (Si) and carbon (C). The carbon atom is linked to three Si atoms in a tetrahedral structure within the bilayer and has a single bond linked to a Si atom in the layer below, as shown in Figure 2.1. The bond length of the nearest neighbour is approximately 1.89 Å and the closest distance between two atoms of the same species in the SiC lattice is approximately 3.08 Å (Zhou et al., 2008).

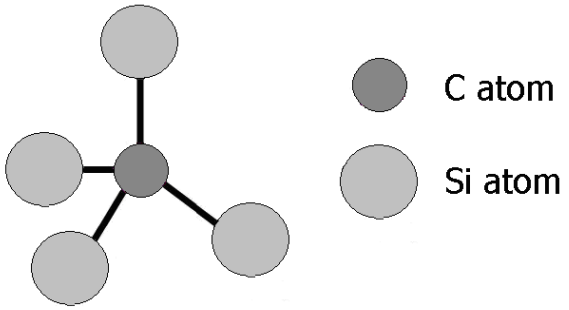

Figure 2.1: Tetrahedral bonding of a C atom with its four nearest Si atoms.

SiC has almost 200 different polytypes due to its different periodic stacking faults as a result of alternate layer arrangement. The most common polytypes are cubic 3C, hexagonal 4H and 6H, as well as rhomboheral 15R, which are differentiated by the repeated stacking sequences of the biatom layers of SiC structure, as shown in Figure 2.2 (Sudarshan, 2006). A, B, C in the figure represent the position of the lattice site of SiC without changing the tetrahedral bonding of the Si-C bilayer. 3C-SiC is also referred as β-SiC whereas the other polytypes are referred as α-SiC. β-SiC can be considered as a low-temperature polytype since it is easier to nucleate and grow while α-SiC is considered as high-temperature polytype that needs relatively high temperatures to grow.

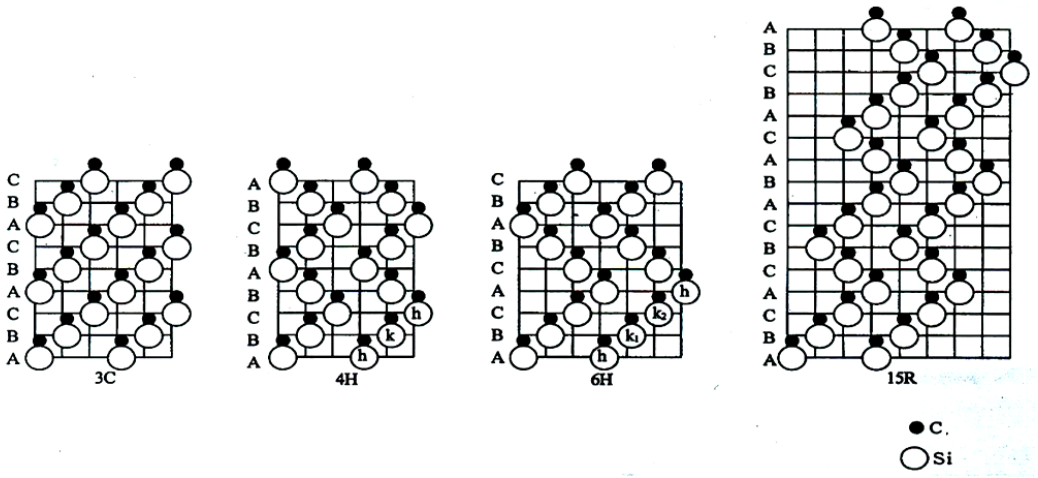

Figure 2.2: Stacking sequence of double layers of 3C, 4H, 6H and 15R-SiC (Sudarshan, 2006).

SiC materials are extremely hard, inert, have wide band gap, high breakdown field strength, high saturation electron drift velocity and depending on doping, the material can be made transparent to optical wavelengths. Table 2.1 shows some of the important properties at room temperature for different polytypes of bulk SiC as well as SiC nanowires (Wong et al., 1997, Powell and Rowland, 2002, Ryu et al., 2005, Fan et al., 2006, Shen et al., 2006, Yan et al., 2006, Zhou et al., 2006a, Chen et al., 2010, Wang et al., 2012).

Table 2.1: Properties for different polytypes of SiC and SiC nanowires at room temperature.

Properties	**3C-SiC (bulk)**	**4H-SiC (bulk)**	**6H-SiC (bulk)**	**3C-SiC nanowires (depending on diameter, D)**
Carrier Concentration (cm^{-3})	~1000 (Zhou et al., 2006a)	~10^{-7} (Zhou et al., 2006a)	~10^{-5} (Zhou et al., 2006a)	0.82 - 1.76 x 10^{7} at V_{ds} = 0.01 and 0.05V (Zhou et al., 2006a)
Energy Gap (eV)	2.4 (Yan et al., 2006)	3.2 (Powell and Rowland, 2002)	3.0 (Powell and Rowland, 2002)	4.42 - 3.31 eV for D = 0.61 - 0.92 nm (Yan et al., 2006)

Table 2.1 (Continued)

Properties	**3C-SiC (bulk)**	**4H-SiC (bulk)**	**6H-SiC (bulk)**	**3C-SiC nanowires (depending on diameter, D)**
Carrier Mobility ($cm^2/V.s$)	1.5	3.2	3.0	6.4 - 15.9 when V_{ds} = 0.01 - 0.05 V (Zhou et al., 2006a)
Field Emission Property ($V\mu m^{-1}$)	N/A	N/A	N/A	4.0 (Ryu et al., 2005) For bamboo-like nanowires, 10.1 at emission current of 10 μAm^{-1} (Shen et al., 2006) 5 and 8.5 at 10 μAm^{-1} and 10 mAm^{-1} (Fan et al., 2006) 2.1 at current density of 10 μAm^{-2} (Chen et al., 2010)
Tensile Strength (GPa)	6.49 ± 0.88 for thin film of thickness 0.40 μm (Wei et al., 2008) 3.16 ± 0.38 for thin film of thickness 1.42 μm (Wei et al., 2008)	0.03448 - 0.137 for bulk ceramic (Shackelford and Alexander, 2000)	0.03448 - 0.1379 for bulk ceramic (Shackelford and Alexander, 2000)	51.5 for D = 0.61 nm (Yan et al., 2006) 53.4 for D = 21.5 - 23.0 nm (Wong et al., 1997) 33.4 for D = ~5 nm (Wang et al., 2012) 12.4 for SiC/SiO_2 nanowires with D =5 nm with oxide thickness = 1 nm (Wang et al., 2012)

From Table 2.1, it can be observed that there is a change in the properties of SiC when its size is reduced to nanometer range. When materials are reduced to nanometer range, it allows the realization of miniaturized devices and systems while providing more functionalities, attainment of high surface area to volume and manifestation of new properties due to quantum confinement effect.

In some cases, the SiC nanostructures were observed to be covered with a layer of amorphous SiO_2 with thickness up to half of the diameter of the SiC cores (10 – 30 nm), forming SiC/SiO_2 core-shell nanostructures (Du et al., 2007, Niu and Wang, 2007a, Wang et al., 2007, Lopez-Camacho et al., 2008, Kim et al., 2009, Yang et al., 2009, Kang et al., 2011, Liao et al., 2012). The presence of an oxide layer had been reported to act as a protective layer against corrosion without affecting the mechanical properties, making them suitable for use as reinforcement in composites. The presence of the oxide layer was also found to enhance the electron emission properties. The improvement in the field emission properties of the core-shell structures, especially in nanowires as compared to conventional SiC nanowires was suggested to be a result of three reasons (Wang et al., 2007). Firstly, high density nanowires had more efficient electron emitting sites, leading to better field emission properties. The wide band-gap SiO_2 shell layer was reported to have a small electron affinity (0.6 – 0.8 eV) that could enhance the field emission of SiC emitters. Finally, the geometry of the core-shell nanowires with high aspect ratio also enhanced the field emission properties by improving the ability of the emitters in controlling the local electric field at the tips. However, there were also some disadvantages of the presence of the oxide shell. The thick oxide shell reduced the electronic conductivity between the nanowires and their contacting electrodes (Li et al., 2002). Aside from that, the different lattice structures of SiC and SiO_2 created thermal stress in the as-synthesized nanostructures due to uneven shrinkage (Li et al., 2002).

2.2.3 Silica (SiO_2)

Silica is an oxide of silicon with the chemical formula SiO_2. It is most commonly found in nature as sand or quartz. The basic building block of the silica molecule consists of a tetrahedral coordination of silica, whereby four oxygen atoms surrounds a central Si atom, as shown in Figure 2.3. The four oxygen atoms in the SiO_4 tetrahedral are shared with other tetrahedral in order to obtain a thermodynamically stable form of silica, yielding the net formula of SiO_2.

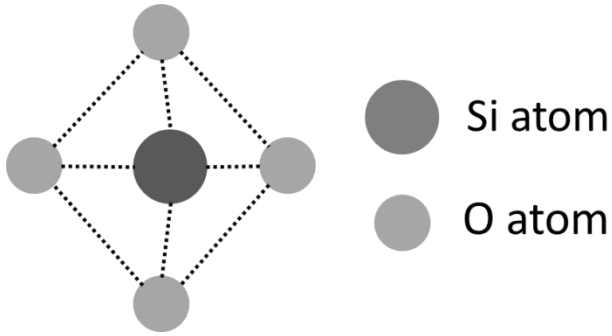

Figure 2.3: Tetrahedral bonding of a Si atom with its four nearest O atoms.

SiO_2 exist in amorphous form as well as in a number of crystalline forms. The crystalline forms involve tetrahedral SiO_4 units linked together by shared O_2 in different Si-O bond lengths and Si-O-Si angles, which result in various polymorphs with the common ones being α-quartz, β-quartz, tridymite and cristobalite. α-quartz is the only stable crystalline form under normal conditions and it is the SiO_2 form that is usually encountered. The difference between the crystalline and amorphous forms of SiO_2 arises in the connectivity of these SiO_4 tetrahedral units. The amorphous form consists of a non-repeating network of tetrahedra, where all oxygen atom corners connect two neighbouring tetrahedra.

Silica is best known for its hardness and inertness. In electronic field, bulk silica is also known as an electric insulator with high chemical stability but when the size is reduced to nanoscale, new properties manifest and the properties of the SiO_2 nanostructures are shown in Table 2.2 (Bilalbegovic, 2006, Ni et al., 2006, Jin et al., 2008, Al-Ruqeishi et al., 2011, Pang et al., 2011).

Table 2.2: Properties of SiO_2 nanowires at room temperature.

Properties	**Value**
Young's Modulus	57 - 93 GPa (Ni et al., 2006)
Electrical conductivity	Varies according to number of Si-O bonds (changes from metallic to insulating as number of bond increases) (Bilalbegovic, 2006)
Fermi level	-3 eV to -7 eV (more positive as number of Si-O chain increases) (Bilalbegovic, 2006)
PL band energies	1.9 – 4.3 eV (Jin et al., 2008, Al-Ruqeishi et al., 2011, Pang et al., 2011)

2.2.4 Synthesis of Si-Based Nanostructures

Due to the unique properties of Si-based nanostructures, many techniques, including top-down and bottom-up approaches, have been developed and applied in the synthesis of Si-based nanostructures (Vaseastha, 2005). The most common methods being chemical vapour deposition (CVD) (Zhang et al., 2001, Chio et al., 2004, Mamails et al., 2004, Yang et al., 2004, Ying et al., 2004, Yang et al., 2005), thermal evaporation (Zhou et al., 1999, Li et al., 2003, Yang et al., 2008b) and carbothermal reduction (Liang et al., 2000a, Meng et al., 2000, Xu et al., 2006). Although these methods are able to produce the nanostructures at lower temperatures and with smaller sizes, these methods have their own problems as compiled by Zhou et al. (2008) in Table 2.3.

Table 2.3: Comparison of several synthesis methods of Si-based nanostructures (Zhou et al., 2008).

Synthesized methods	Yield	Cost	Temperature (°C)	Diameter (nm)	Catalyst
Carbon-nanotube confined reaction	Low	Higher	1,400	20 – 25	No
Arc discharge	Higher	Low	3,000	20 – 60	Yes
Laser ablation	High	High	900	20 – 70	Yes
Sol-gel and carbothermal reduction	Higher	Lower	900	40 – 80	No
Chemical vapour deposition method	Higher	Higher	1,100	10 – 100	Yes
High-frequency induction heating	Higher	Lower	1,450	5 – 20	No

The methods listed in Table 2.3, aside from laser ablation and sol-gel method, all required high temperatures, which posed a problem in the commercialization of these methods in producing Si-based nanostructures as a result of the high cost incurred. Although laser ablation and sol-gel method could be performed at lower temperatures, the systems are complex and require expensive raw materials and these contributed to high production cost (Narciso-Romero and Rodriguez-Reinoso, 1996). Here, two routes are reviewed in the growth of Si-based nanostructures, namely direct growth on Si substrate and pyrolysis of biomass. Direct growth on Si substrates refers to the growth of Si-based nanostructures on Si substrate. Several techniques have been used in the direct growth route, which include CVD and carbothermal reduction. In the pyrolysis of biomass, the method normally employed is the carbothermal reduction. The two routes chosen here differ in terms of the different growth mechanism, where one involves the growth of nanostructures on a substrate while the other involves the growth of stand-alone nanostructures.

2.3 Direct Growth of Si-Based Nanostructures on Si Substrate

The direct growth method involved the growth of Si-based nanostructures using only Si substrate on the Si substrate without using any external source except for carbon sources in the synthesis of SiC nanostructures. The ability to grow these nanostructures directly on Si substrate offered the possibility of direct integration of these nanostructures for electronic device building. This attracted various researches being performed on it. From previous works, it was found that different types of products were formed such as SiC nanorods or nanowires, core-shell SiC/SiO_2 nanowires, core-shell SiC/a-C nanowires, SiO_2 nanowires and carbon nanotubes using this method under different parameters. The effects of these parameters such as starting materials, growth temperature, catalyst, furnace atmosphere and cooling rate will be described in the following subsections.

2.3.1 Effect of Starting Materials

2.3.1.1 Si source

Si wafer is a good alternative in producing Si-based nanostructures as it acts as a Si source and simultaneously as a substrate in collecting the nanostructures without requiring additional Si sources. In addition, by controlling certain parameters, it is possible to control the growth location of nanostructures on the Si wafer, enabling selective patterning for electronic device building.

Introduction of a thin silicon oxide (SiO_x) layer on the Si substrate by either thermal oxidation (Park et al., 2007, Jeong et al., 2008) or thermal evaporation using SiO powder (Li et al., 2002) had been found to enhance the growth of Si-based

nanostructures. Different thicknesses of the oxide layer would lead to different nanostructures formed. Thin layers of oxide (< 150 nm) were found to be beneficial for the growth of SiC nanostructures (Li et al., 2002) while thick layers of oxide (500 nm) were found to be more suitable for growth of SiO_2 nanostructures (Jeong et al., 2008). However, if the oxide layer was too thick (> 3 μm), it would inhibit the growth of Si-based nanostructures (Park et al., 2007). SiC nanowires were found growing on the bare Si substrate while no nanostructures were found in regions grown with 3 μm SiO_2.

Presence of defects had also been reported to have a large influence on the growth of Si-based nanostructures on the Si substrate. The defects were introduced on the Si substrate surface by mechanical scratching (Liao et al., 2012) or etching (Park et al., 2007). They acted as nucleation sites and promoted the growth of nanostructures, especially on the [111] planes exposed by the grooves or ledges created by the defects due to their lowest surface energies. This resulted in higher amount of SiC nanowires with average diameter of 30 nm and length of tens of μm being found in the scratched regions as opposed to the unscratched regions (Liao et al., 2012).

Placement of Si substrate in the experimental setup is another important factor in the synthesis of Si-based nanostructures using direct growth method. It was found that SiC nanostructures were found only if the Si substrate was placed downstream from the carbon source in order for the carbon species to be deposited onto the Si substrate (Baek et al., 2006, Al-Ruqeishi et al., 2010). The distance between the carbon source and the Si source also affected the morphologies of the nanostructures formed. Al-Ruqeishi et al. (2010) reported the growth of β-SiC nanowires by exposing the silicon substrate to graphite powder that was placed upstream of the tube furnace. Different Si substrates were placed at certain distances from graphite source and its effects were

studied. High yield of β-SiC nanowires formed at locations near the graphite source with the maximum yield at a distance of 2 cm and 4 cm. The yield started to decrease with increasing distance. At the location far from the graphite source (10 cm), SiC nanowires were only found at the edges of the Si substrates where defects such as grooves and ledges existed. The nanowires on the Si substrate at locations near the graphite source were also reported to have larger diameters with the diameter range of 40 nm to 500 nm. The reason for the higher yield and larger diameters at locations close to the graphite powder was because of the higher reactant species available at these regions that allowed continuous growth of nanowires.

2.3.1.2 Carbon Source

Different forms of carbon source had been reported in the growth of SiC nanostructures using direct growth on Si substrate. The Si substrate was either exposed to solid carbon that were placed upstream of the Si substrate such as carbon powder (Ryu et al., 2004, Baek et al., 2006, Niu and Wang, 2007b, Wang et al., 2007), graphite (Li et al., 2002, Al-Ruqeishi et al., 2010), detonation soot powders (Yang et al., 2009) and charcoal powders (Du et al., 2007) or gaseous form of carbon such as ethanol (Yang et al., 2008a, Kim et al., 2009), methane (Lopez-Camacho et al., 2008, Panda and Jacob, 2009, Liao et al., 2012), ferrocene (Niu and Wang, 2007a), carbon monoxide (CO) (Attolini et al., 2008) and hexamethyldisilane (HMDS) (Panda et al., 2010). The gaseous carbon source was found to require lower growth temperatures of 1000°C – 1100°C as compared to the solid carbon source with growth temperatures ranging from 1200°C – 1500°C (Lopez-Camacho et al., 2008, Kim et al., 2009). Growth using solid carbon

might require a higher growth temperature due to the need to decompose the solid carbon first in order to form gaseous carbon species.

The concentration of the carbon source was found to play an important role as well in determining the final structures of the products. Different products from SiC/SiO_2 core-shell nanowires to SiC/C core-shell nanowires or carbon nanotubes were reported when the methane concentration was increased. Liao et al. (2012) reported the growth using catalyst-assisted chemical vapour reaction by exposing the Si substrate to ferrocene and methane under H_2 flow at 1100°C for 10 mins. The ferrocene acted as the catalyst, producing Fe particles that deposited onto the Si substrate surface. At methane concentrations less than 5%, only SiC/SiO_2 core-shell nanowires were formed as opposed to carbon nanotubes that were formed at methane concentrations more than 5%. The reason for different products formed was related to the different catalyst particles formed. When heated at high temperature, decomposition of ferrocene and methane occurred. If methane concentration was low, the Fe particles would deposit on the Si substrate and diffused into the SiO_2 layer to the interface between SiO_2 and Si in order to form iron silicide (FeSi) that would later induced the growth of SiC/SiO_2 core-shell nanowires. When the methane concentration was more than 5%, the carbon species would also deposit onto the Si substrate surface and diffused through the SiO_2 layer to the interface between SiO_2 and Si. Instead of FeSi, iron carbide was formed and induced the growth of carbon nanotubes.

There was also another report on the effect of methane concentration (Lopez-Camacho et al., 2009b). In their chemical vapour deposition (CVD) method, they exposed the Ni-coated substrates to methane under H_2 at 950°C for 10 mins. They found that SiC/SiO_2 core-shell nanowires were formed when the methane concentration was between 12% and 45% but when the methane concentration was further increased to

concentrations between 59% and 75%, SiC/a-C core-shell nanowires was formed instead, whereby the SiC nanowires were encapsulated by an amorphous carbon layer. The evolution of the nanostructures from SiC/SiO_2 to SiC/a-C when methane concentration was increased had been reported to be a result of the change in the growth mechanism from vapour-liquid-solid (VLS) to solid-liquid-solid (SLS). When carbon concentration was increased further, a layer of carbon would be deposited onto the Si substrate and this C layer would hinder the VLS mechanism between SiO, C and Ni nuclei. The Si source would have to diffuse through the solid surface into the Ni and reacted with the C layer. Since the nuclei was surrounded by the C layer, SiO_2 shell could not be formed when the SiC nanowires precipitated out from the nuclei but instead be encapsulated by the amorphous C layer.

2.3.2 Effect of Growth Temperature

The growth temperature is another important parameter in the synthesis of Si-based nanostructures. It was found to be highly dependent on the source materials, ambient and incorporation of catalyst, which will be described in their respective sections. The normal growth temperature using direct growth method in synthesizing Si-based nanostructures ranged from 1100°C – 1550°C. The growth temperature was also found to affect the morphologies and yield. An increase in growth temperature from 1050°C to 1100°C led to a change of structure from nanowires with diameters less than 80 nm to rods with diameters of 2 μm (Attolini et al., 2008). An increase in the growth temperature from 900°C to 1100°C was also reported to cause a change in the product from carbon nanotubes to SiC/SiO_2 core-shell nanowires when the Si substrate was exposed to methane and ferrocene was used as catalyst source (Liao et al., 2012).

2.3.3 Effect of Catalyst

Addition of catalyst in the system was also found to have an effect on the growth of Si-based nanostructures. Catalysts could be defined as substances that were added into the system to change the rate of reaction by participating in the multiple chemical transformations. It promoted the growth of nanostructures by lowering the free energy of activation through different routes of chemical reactions, enabling the growth of nanostructures to proceed at lower temperatures with higher yield. Growth of Si-based nanostructures had been reported to be possible at lower temperatures of 950°C to 1100°C when catalysts were incorporated into the system (Wang et al., 2007, Lopez-Camacho et al., 2009a) as compared to systems without catalysts with the normal growth temperature range of 1200°C-1550°C (Niu and Wang, 2007a). However, the metal catalysts that remained on the nanostructures were also considered as impurities that limited the applications of these nanostructures (Kang et al., 2011).

Here, various types of catalysts had been used such as $Ni(NO_3)_2$ (Ryu et al., 2004, Attolini et al., 2008, Kim et al., 2009, Al-Ruqeishi et al., 2010), Cr (Li et al., 2002), Ni (Lopez-Camacho et al., 2008), Fe from ferrocene (Niu and Wang, 2007a, Liao et al., 2012), Fe_3O_4 (Wang et al., 2007), WO_3 (Ryu et al., 2004, Baek et al., 2006) and ZnS (Niu and Wang, 2009). The catalysts were introduced into the system by dipping the Si substrate into an ethanol solution containing the catalysts (Attolini et al., 2008, Al-Ruqeishi et al., 2010), placing the catalyst powder upstream from the Si substrate (Niu and Wang, 2007a, Liao et al., 2012) or by sputtering a layer of catalyst on the Si substrate surface (Lopez-Camacho et al., 2008).

When using catalysts in the growth of Si-based nanostructures, the mechanism had always been correlated to the VLS mechanism, whereby the metal catalyst particles

formed metal silicide and acted as nuclei which absorbed the reactant species from surrounding gases. Upon supersaturation, the nanostructures would precipitate out (Ryu et al., 2004, Attolini et al., 2008, Lopez-Camacho et al., 2008, Kim et al., 2009, Al-Ruqeishi et al., 2010). Nanostructures grown using catalysts under VLS mechanism had also been noted with metallic droplets on the tips of the nanostructures though in some cases, the metallic droplets were found at the base of the nanostructures and this growth mechanism was named as base-growth mechanism (Li et al., 2002, Niu and Wang, 2007a, Liao et al., 2012).

In some cases, the catalyst particles only initiated the decomposition process of silicon and carbon source so as to enhance the reaction rate such as ZnS (Niu and Wang, 2009) and WO_3 (Ryu et al., 2004, Baek et al., 2006). Upon completion of process, the catalyst particles would have been evaporated without having any effects on the nanostructures formed. Niu and Wang (2009) evaporated ZnS powder on Si substrate. The use of sulfide was very important in the growth of nanowires. The Si vapour evaporated from Si substrate reacted with vapour phase of S or SO_2 from ZnS forming SiS vapour. Si then precipitated out from SiS and formed nucleus for the growth of nanostructures. In the case of WO_3, it was used to provide CO source through carbothermal reduction of WO_3.

2.3.4 Effect of Furnace Atmosphere

The atmosphere inside the furnace during the synthesis process was also found to affect the growth kinetics of the nanostructures. The atmosphere inside the furnace was introduced for several reasons, either to provide an inert atmosphere to remove unwanted species, to provide a reductive atmosphere for carbothermal reduction or to

act as carrier gas for the reactant species. The functions of different atmospheres would be described in the following parts.

A low partial pressure of oxygen (O_2) in the furnace atmosphere was found to be beneficial in the growth of SiC nanostructures but if the partial pressure of O_2 was too high, it would inhibit SiC growth and favored the growth of SiO_2 nanostructures (Du et al., 2007). The growth of nanostructures under O_2 was related to the oxide-assisted growth (OAG) mechanism (Zhang et al., 2003), whereby the O_2 played an important role in the formation of SiO_2 or SiC. O_2 would react with Si, forming SiO species that later transformed into SiC or SiO_2 species depending on the partial pressure.

Argon (Ar) was commonly used in the synthesis process as a carrier gas for the reactant species (Li et al., 2002). It was also used to provide an inert atmosphere in the furnace chamber (Li et al., 2002, Yang et al., 2008a). Ar was introduced into the furnace in order to remove unwanted species and stabilize the Ni catalysts deposited on the Si substrate surfaces, preventing the oxidation of the catalyst particles that would hinder the functions of catalysts (Lopez-Camacho et al., 2008, Lopez-Camacho et al., 2009a). However, it was reported that Ar had lower efficiency in removing O_2. Residual O_2 still existed in the furnace chamber and would lead to preferential growth of SiO_2 nanowires (Lopez-Camacho et al., 2008). The flow rate of the Ar gas must also be controlled in growing the nanostructures. When synthesizing SiC nanostructures, the carbon source had to dissociate into CO species in order for SiC formation reactions to take place. If the Ar flow was too high, it would either remove the carbon source from the reaction zone or transfer the carbon source to the reaction zone without being oxidized into CO and this would lead to the deposition of carbon nanoparticles on the nanowires, as observed in the nanowires formed by Kim et al. (2009).

Hydrogen (H_2) was normally used to provide a reductive atmosphere in the furnace chamber and it was found to have a higher efficiency in removing residual O_2 in the furnace chamber as compared to Ar to produce an O_2 deficient zone for the growth of SiC nanostructures (Lopez-Camacho et al., 2008). However, it was also reported that the presence of H_2 prevented the growth of SiC nanostructures on SiO_2-coated Si substrates (Park et al., 2007). When heated at high temperature, H_2 dissociated into H species that preferentially adsorbed onto the SiO_2 surface and bonded with the Si dangling bonds whereas the carbon species preferentially adsorbed onto the bare Si substrate and reacted with the Si dangling bonds. The H species on the SiO_2 surface prevented incoming carbon species to react with Si and thus resulted in no SiC nanostructures being formed on the SiO_2 surface while SiC/SiO_2 core-shell nanowires were found on the bare Si substrate. This enabled selective patterning of SiC nanostructures on Si substrate by using a thick layer of SiO_2 and exposing the substrate to H_2 atmosphere. Although the growth of SiC/SiO_2 nanowires was reported to be possible under H_2 atmosphere, the pressure had to be controlled within a narrow range of 375 Torr to 600 Torr (Lopez-Camacho et al., 2008). A pressure of 375 Torr showed the optimum results in terms of high yield and considerable length. As the pressure was increased to 600 Torr, SiC/SiO_2 core-shell nanowires were still formed but with the presence of another side product of SiO_2 nanowires. The lengths of the nanowires were also visibly shorter as compared to that of 375 Torr. This is because the high pressure would suppress the catalytically activated decomposition reaction of methane and decrease the amount of C species available for SiC growth, thus slowing down the growth rate of SiC. The remaining oxide species would then favored the growth of SiO_2 nanowires.